Materials and Design 80 (2015) 63–69

Contents lists available at ScienceDirect

Materials and Design

journal homepage: www.elsevier.com/locate/matdes

Microstructural evolution of the interface between NiCrAlY coating and superalloy during isothermal oxidation

Y.Z. Liu [a,b], X.B. Hu [b], S.J. Zheng [b,*], Y.L. Zhu [b], H. Wei [c], X.L. Ma [b,*]

[a] School of Chemistry and Materials Science, University of Science and Technology of China, Hefei 230026, PR China
[b] Shenyang National Laboratory for Materials Science, Institute of Metal Research, Chinese Academy of Sciences, Shenyang 110016, PR China
[c] Superalloys Division, Institute of Metal Research, Chinese Academy of Sciences, Shenyang 110016, PR China

ARTICLE INFO

Article history:
Received 19 January 2015
Revised 7 April 2015
Accepted 5 May 2015
Available online 6 May 2015

Keywords:
Coating
Superalloy
Isothermal oxidation
Interface
Transmission electron microscopy (TEM)

ABSTRACT

NiCrAlY coating was plasma-sprayed on a Ni-based single crystal superalloy and then subjected to isothermal oxidation at 1100 °C in air up to 50 h. Using scanning electron microscopy (SEM) and transmission electron microscopy (TEM), we investigate interfacial microstructure evolution of the coating induced by internal oxidation and nitridation. After 5 h oxidation, α-Al_2O_3 and Cr_2O_3 sub-layers form at the coating/substrate interface. Interestingly, after 10 h oxidation, pure Al phase is found at the coating/substrate interface owing to decomposition of substrate phase γ′-Ni_3Al. Although, after 25 h oxidation, hexagonal AlN and cubic TiN form in the substrate close to the coating/substrate interface, after 50 h oxidation, AlN transforms into α-Al_2O_3 owing to internal oxidation while TiN remains in the substrate because of its high stability. The findings of this work provide solid experimental evidence of microstructural evolution at the coating/substrate interface, especially demonstrate the conjecture that pure metal phases and nitrides could precipitate at coating/substrate interface after high temperature oxidation.

1. Introduction

MCrAlY-typed (M = Fe, Co, Ni, or Ni + Co) coatings with good balance between oxidation-resistance, anticorrosive, and mechanical properties, are commonly applied as standalone coatings or as bond coats in thermal barrier coating (TBC) systems in the fields of aerospace propulsion, power generation and marine propulsion [1,2]. NiCrAlY coatings can improve oxidation resistance of Ni-based superalloys via formation of dense α-Al_2O_3-rich layers on the coating surfaces and at the coating/superalloy interfaces. The dense α-Al_2O_3-rich layers provide protection against rapid degradation of coated superalloys by virtue of restraining the diffusion-controlled oxidation [3]. However, failure of coating systems often starts from the coating/superalloy interfaces due to different thermal expansion coefficients between the coatings, oxide layers and the substrates [4]. Moreover, in long-term service at an elevated temperature, Kirkendall voids, oxides, and intermetallic compounds formed at the coating/substrate interfaces could remarkably degrade mechanical properties of the coating systems [5,6]. Improvement of coating systems needs in-depth understanding of microstructural evolution of coating/substrate interfaces, unfortunately, which has been hitherto lacking.

Microstructural evolution of MCrAlY-type coating systems have been investigated via X-ray diffraction (XRD), scanning electron microscopy (SEM), and energy dispersive spectroscopy (EDS) [7–14]. For instance, based on SEM observation, Hasegawa et al. found that an interdiffusion zone formed between a NiCrAlY coating and a Ni-based superalloy after oxidation at 1413 K for 10 h and 50 h, and in the interdiffusion zone β-NiAl which was one of two main phases in the NiCrAlY coating disappeared [7]. Also, oxides such as Y_2O_3, $YAlO_3$, and $Y_3Al_5O_{12}$ particles were identified with XRD and SEM at NiCoCrAlY coating/superalloy interfaces [8]. Furthermore, using XRD, SEM, and EDS, Zhang et al. found Cr-rich and W-rich carbides formed between a NiCrAlYSi coating and a K40S superalloy during oxidation at 1323–1423 K [9]. Besides, other precipitates were also discovered, for instance, Cr, Co, Mo-rich particles and Ta, Hf, Si-rich particles between a NiCoCrAlYHfSi coating and a single crystal superalloy 1484 after 200 h exposure at 1100 °C [10], and Cr(W)-rich σ precipitates between a NiCoCrAlYSi coating and a Nickel-based single crystal superalloy after oxidation for up to 300 h at 1100 °C [11]. Except for precipitated particles, Kirkendall voids can be often seen. For example, a porous layer composed by TiO_2 and $NiCr_2O_4$ mixture was found in the interdiffusion zone between a NiCrAlY/CrON

* Corresponding authors.
E-mail addresses: sjzheng@imr.ac.cn (S.J. Zheng), xlma@imr.ac.cn (X.L. Ma).

http://dx.doi.org/10.1016/j.matdes.2015.05.014
0261-3069/

duplex coating and a DSM11 superalloy substrate after thermal treatment at 1100 °C for 100 h in static air [12–14].

Although the above literatures [7–14] have provided a big picture of microstructural evolution, details especially induced by internal oxidation and nitridation at the coating/substrate interface during the initial stages of oxidation, such as what phases first precipitate and how they transform, are still unclear due to detection limits of XRD and SEM. Transmission electron microscopy (TEM) without limitations of contents and sizes of precipitates has been rarely used for microstructural investigation in NiCrAlY coating systems mainly due to the difficulty in cross-sectional TEM specimen preparation [15]. Consequently, uncertainties still exist over the detailed microstructure evolution at the coating/substrate interfaces, especially the oxide layer/substrate interface, during high temperature oxidation. For instance, Warnes et al. [16] and Li et al. [17] inferred that β-NiAl and γ′-Ni_3Al can decompose to form Al at high temperature, but it has not been experimentally illustrated so far. As products of internal nitridation, Litz et al. [18] only found TiN while Krupp and Christ [19] detected both AlN and TiN simultaneously in the superalloys with approximately equal contents of Al and Ti after 100 h oxidation at 1000 °C in air. This discrepancy might result from only studying a stage but not a whole oxidation process or missing phases with small contents. Hence, it is necessary to systemically study the microstructural evolution of the interface between the NiCrAlY coating and the substrate at as more as stages during the oxidation process using TEM.

In this paper, a combination of SEM, TEM, scanning transmission electron microscopy (STEM), and energy dispersive X-ray microanalysis (EDX) is used to investigate the microstructural evolution at the NiCrAlY/substrate interface during isothermal oxidation at 1100 °C. The results can clarify the interfacial microstructural evolution, particularly phases involved N, O, Al, Ti and Cr in the vicinity of the coating/substrate interface. Additionally, possible influences of the microstructural evolution on performance of the coating and insights on design of new MCrAlY coating systems are discussed.

2. Experiments

At the beginning, grit-blasting was carried out on the substrate surface to improve the adhesive strength between the coating and the substrate. Via a vacuum plasma spray (VPS) system, Amdry962 (Ni–22Cr–10Al–1Y, wt.%) powder was sprayed onto a Ni-based single crystal superalloy with a composition of 8Co–8Cr–8W–6Ta–5Al–1Ti (wt.%). The thicknesses of the as-sprayed NiCrAlY coatings are 90–120 μm. Spray parameters used to synthesize the NiCrAlY coatings are given in table 1.

The isothermal oxidation of the coated samples was carried out in a SNOL 4/1100LSC01 furnace at 1100 °C in static air for up to 50 h. During the isothermal oxidation, the coated samples were mounted in crucibles and put into the furnace at room temperature (22 ± 0.5 °C), then heated to 1100 °C in 40 min. After each holding time, more than 5 samples were removed from the furnace and freely cooled down in air.

Table 1
Spray parameters for NiCrAlY coating.

Spray parameters	NiCrAlY
Current (A)	500
Voltage (V)	125
Pressure of primary gas Ar (MPa)	0.52
Pressure of second gas H_2 (MPa)	0.45
Flow rate of primary gas Ar (m^3/h)	2.83
Flow rate of second gas H_2 (m^3/h)	0.42
Powder feeding rate (g/min)	30
Spray distance (mm)	150
Pressure of the spraying chamber (Pa)	$(5–8)\times10^3$

The TEM samples used for cross-sectional microstructure study were prepared by the conventional mechanical thinning and ion milling. The samples were cut and then ground using 5000 grit SiC paper, followed by polishing with diamond slurry up to a 0.5 μm finish. Polished surfaces were first cleaned by deionized water and then by ultrasonic cleaning in acetone and ethanol. After dimpling, ion milling was performed on a Gatan precision ion polishing system (PIPS). Conventional TEM investigation and STEM-EDS analysis were conducted using a FEI Tecnai G^2 F30 equipped with a high-angle annular dark-field (HAADF) detector. Low magnification morphology was analyzed by a FEI Inspect F50 SEM.

3. Results and discussion

3.1. Microstructures of the as-sprayed coating system

Atypical cross-sectional micrograph and main phases of the as-sprayed NiCrAlY coating are presented in Fig. 1. It is clearly seen that the average thickness of the coating is about 105 μm (Fig. 1a). Because of grit-blasting which was performed on the substrate surface to improve the adhesive strength between the coating and the substrate, the coating/substrate interface fluctuates. Based on the SEM and TEM results, it can be concluded that the NiCrAlY coating mainly consists of γ-Ni (marked with "A" in Fig. 1b) and β-NiAl (marked with "C" in Fig. 1b), as well as a small amount of α-Cr precipitates (marked with "B" in Fig. 1b). Typical selected area electron diffraction (SAED) patterns corresponding to these phase are shown in Fig. 1c–e. The superalloy used in this study contains master phase γ-Ni and strengthening phase γ′-Ni_3Al demonstrated by SAED pattern of $[1\,1\,1]_{\gamma'\text{-}Ni3Al}$ in Fig. 1f.

3.2. Formation of Cr_2O_3 and α-Al_2O_3 sub-layers (5 h oxidation)

After 5 h oxidation at 1100 °C, an oxide layer with a local maximum thickness of about 5 μm forms at the coating/substrate interface (Fig. 2a). A TEM image in Fig. 2b shows that the oxide layer presents two sub-layers. The upper one, which is adjacent to the coating and marked with "A", is mainly composed of Cr_2O_3. While the lower one, which is close to the substrate and labeled with "B" consists of α-Al_2O_3. Also, Kirkendall voids can be seen in the sub-layers as illustrated in Fig. 2b.

As the reasons for formation of the Cr_2O_3 and α-Al_2O_3, it can be ascribed to the selective internal oxidation. O reacts with Al and Cr to form stable metal oxides due to high affinity of O with metal elements, for example, the O affinity to Al is ΔH_f^{θ} (Al_2O_3) = 1675.7 kJ/mol and that O to Cr is ΔH_f^{θ} (Cr_2O_3) = 1139.7 kJ/mol [20]. Possibly, α-Cr and solid-soluted Cr in the γ-Ni of the coating react with the O by the following reactions:

$$2\alpha\text{-Cr} + 3[O] \rightarrow Cr_2O_3 \quad (1)$$

$$2[Cr] + 3[O] \rightarrow Cr_2O_3 \quad (2)$$

Oxidation of Al-containing phases, such as β-NiAl (Fig. 1e) in the as-sprayed NiCrAlY coating or γ′-Ni_3Al (Fig. 1f) in the substrate close to the coating/substrate interface, will result in formation of α-Al_2O_3 (Fig. 2b) by the following reactions,

$$2\beta\text{-NiAl} + 3[O] \rightarrow Al_2O_3 + 2Ni. \quad (3)$$

$$2\gamma'\text{-}Ni_3Al + 3[O] \rightarrow Al_2O_3 + 6Ni. \quad (4)$$

The formation of the sub-layers mainly results from the different contents, diffusivity and oxides formation energy between Al and Cr, as well as protective effect of the external oxide layer. As

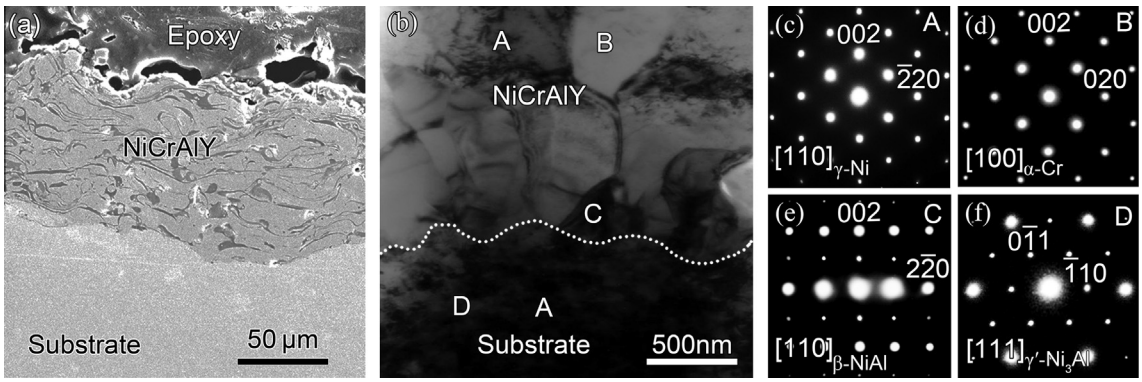

Fig. 1. Typical microstructure and main phases of the as-sprayed NiCrAlY coating: (a) second electron image (SEI) of integrate cross-sectional microstructure, (b) bright field (BF) image of the interface between the coating and the substrate, (c) selected area electron diffraction (SAED) of γ-Ni which is took from [1 1 0] zone axis, (d) SAED of α-Cr which is took from [1 0 0] zone axis, (e) SAED of β-NiAl which is took from [1 1 0] zone axis and (f) SAED of γ′-Ni_3Al which is took from [1 1 1] zone axis.

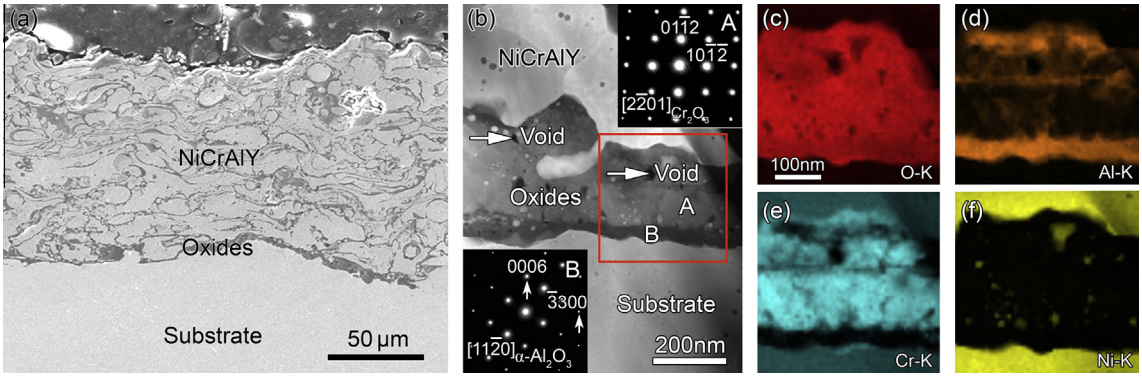

Fig. 2. Typical microstructure and chemical composition of the NiCrAlY coating after oxidation at 1100 °C for 5 h: (a) SEI of integrate cross-sectional microstructure; (b) high angle annular dark field (HAADF) image of the interface between the coating and the substrate, and the SAEDs of main phases in the interfacial oxides layer which are took from [2 $\bar{2}$ 0 1] and [1 1 $\bar{2}$ 0] of Cr_2O_3 and α-Al_2O_3, respectively, (c)–(f) STEM-EDS maps of O, Al, Cr and Ni, respectively.

for α-Al_2O_3 sub-layer locates beneath the Cr_2O_3 sub-layer in the oxide layer, it is very possibly because of the large difference of the formation energies between α-Al_2O_3 and Cr_2O_3. The molar Gibbs free energies $\left(DeltaG_f^o\right)$ for formation of α-Al_2O_3 and Cr_2O_3 at 1100 °C are −1328 kJ/mol and −763 kJ/mol, respectively [20]. Hence, α-Al_2O_3 can form under a lower oxygen partial pressure (P_{O_2}) than that for Cr_2O_3. Additionally, at the beginning of oxidation, O rapidly reacts with Al, Cr and Ni on the coating surface to form an external oxide layer consisting of a mixture of Al_2O_3, Cr_2O_3, and NiO [5]. With protection of the external oxide layer, penetration of O to the coating/substrate interface becomes difficult. So that the partial pressures of oxygen in the interface zone is too low to form Al_2O_3 and Cr_2O_3 simultaneously, and only high enough for that O react with Al to form α-Al_2O_3 layer. In this way, α-Al_2O_3 grows into a dense and continuous layer. With depletion of Al during the oxidation, the residual oxygen concentration in the interface zone increases gradually and become high enough for formation of Cr_2O_3, then Cr_2O_3 starts to grow. After oxidation at 1100 °C for 5 h, Cr_2O_3 also grows to a continuous layer. Considering that the content of Cr is greater in the NiCrAlY coating than that in the substrate and the early formed α-Al_2O_3 sub-layer can impede O diffusion into substrate, Cr_2O_3 sub-layer forms above the α-Al_2O_3 sub-layer. Moreover, the content of Cr (27 wt.%) in the coating is more than that of Al (11 wt.%), Cr_2O_3 takes larger proportion of the interfacial oxide layer than that of α-Al_2O_3 (Fig. 2b). So far it can be well understood that why the interfacial oxide layer presents an upper Cr_2O_3 sub-layer with large thickness and a lower α-Al_2O_3 sub-layer with small thickness. At last, it is also worth noting that the sub-layers preserve in all the oxidation durations performed in this work.

3.3. Precipitation of pure Al (10 h oxidation)

After oxidation for 10 h at 1100 °C, some strip or parallelogram shaped Al grains precipitate adjacent to the oxide layer (Fig. 3). via STEM-EDS (Fig. 4b, d and h) and SAED (inset in Fig. 4a) analysis, the Al grain marked with "A" in Fig. 4a can be identified as face centered cubic (fcc) Al which is in [1 0 0] direction. The precipitated Al grain also contains a few particles comprising Ti (Fig. 4e) and Ni (Fig. 4g) simultaneously.

The pure Al may greatly degrade the mechanical properties of the coating due to its low strength compared to the NiCrAlY coating. Therefore, it is imperative to investigate the formation mechanism of the pure Al. As shown in Fig. 4a, the Al grain is embedded in the substrate, indicating that the Al phase should result from decomposition of substrate phases. It has been reported that during oxidation at temperatures above 1000 °C, γ′-Ni_3Al can decompose into γ-Ni and Al [17]:

$$2\gamma'\text{-}Ni_3Al \rightarrow 6\gamma\text{-}Ni + 2[Al] \quad (5)$$

In our case, the γ′-Ni_3Al also contains little solution element Ti. Therefore, when γ′-Ni_3Al decomposes, particles containing Ti (Fig. 4e) and Ni (Fig. 4g) precipitate in the Al phase since solubility of Ti and Ni in Al are only ~0.2 at.% [21] and ~0.11 at.% [22],

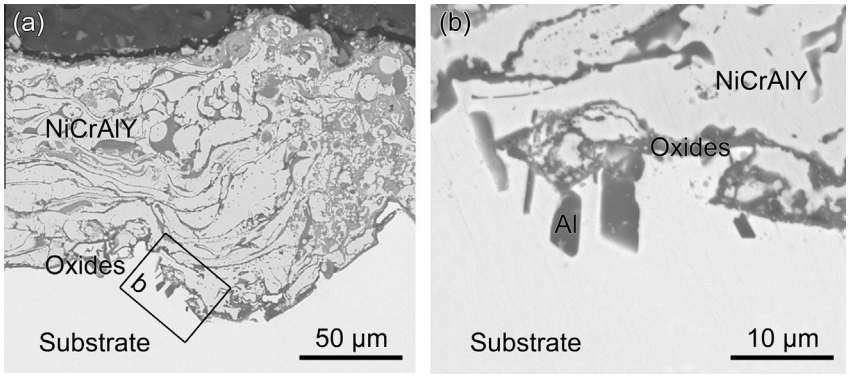

Fig. 3. Cross-sectional microstructures of the coating oxidized at 1100 °C for 10 h: (a) backscatter electron image (BEI) of the integrate coating system, (b) local magnified image of the zone marked with "b" in (a), it clearly shows some Al grains precipitate next to the interfacial oxides.

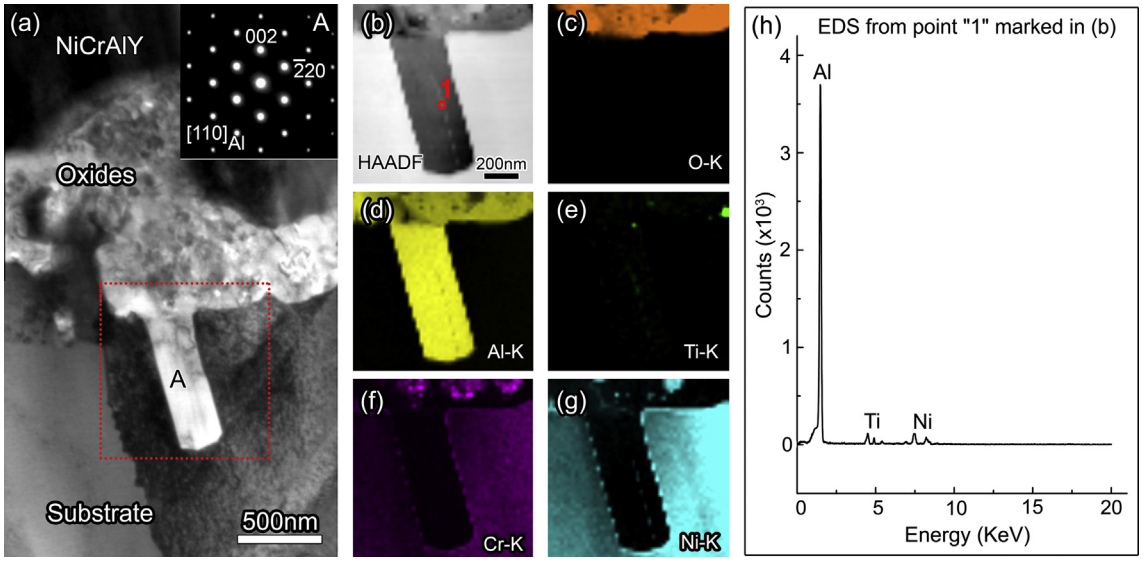

Fig. 4. Microstructure and chemical composition at the coating/substrate interface after oxidation at 1100 °C for 10 h: (a) BF image of the coating/substrate and SAED of $[1\,1\,0]_{Al}$ from the precipitate marked with "A", (b) HAADF image including partial oxides layer and the precipitate marked with "A" in (a), (c)–(g) STEM-EDS maps of O, Al, Ti, Cr and Ni, respectively, and (h) EDS from point "1" marked in (b).

respectively. Additionally, decomposition of γ′-Ni_3Al will cause detrimental effect on the overall performance of the coating system, because the γ′-Ni_3Al is the key strengthening phase in the superalloys.

3.4. Formation of AlN and TiN (25 h oxidation)

In comparison with the 5 h and 10 h oxidation, the coating and the substrate are internally oxidized (Fig. 5a) after oxidation at 1100 °C for 25 h. Polyhedron shaped AlN and spot shaped or short rod-like TiN form in the substrate adjacent to the oxide layer (Fig. 5b). Authenticated with STEM-EDS (Fig. 6a–e, h and i) and SAED (Fig. 6f and g), precipitates marked with "A" and "B" in Fig. 6a can be indexed as fcc-TiN orientated in [100] zone axis (Fig. 6f) and hexagonal close-packed (hcp) AlN aligned in $[2\,\bar{1}\,\bar{1}\,0]$ zone axis (Fig. 6g), respectively.

There has been hardly any report about precipitation mechanism of hcp-AlN and fcc-TiN in NiCrAlY coated Ni-based superalloys. Here, we suggest that the nitride phases result from nitridation of Al formed after 10 h oxidation (Fig. 4) and nitridation of solution element Ti in the matrix γ/γ′. Chemical reactions can be described using the following equations:

$$[Al] + [N] = AlN \tag{6}$$

$$[Ti] + [N] = TiN \tag{7}$$

A raising question here is why nitrides not oxides form in the substrate. As we observed in the samples with shorter oxidation durations, oxidation is more energetically favorable than nitridation since oxides such as α-Al_2O_3 have more negative formation energy than that of nitrides such as AlN [20]. However, the oxidation of the coating and the formation as well as growth of oxide layer consume most of the O, in other words the coating and the oxide layer keep the substrate away from O. In contrast, N without consumption can penetrate the coating and the oxide layer, and react with solid-soluted Al and Ti to form AlN and TiN. Another apparent reason for formation of TiN in the substrate is that Ti is only alloying element in the substrate, but not the NiCrAlY coating.

3.5. Transformation of AlN into α-Al_2O_3 (50 h oxidation)

Through massive investigations, we find hcp-AlN disappear while α-Al_2O_3 form instead in the substrate next to the coating/substrate interface after oxidation at 1100 °C for 50 h, at the mean

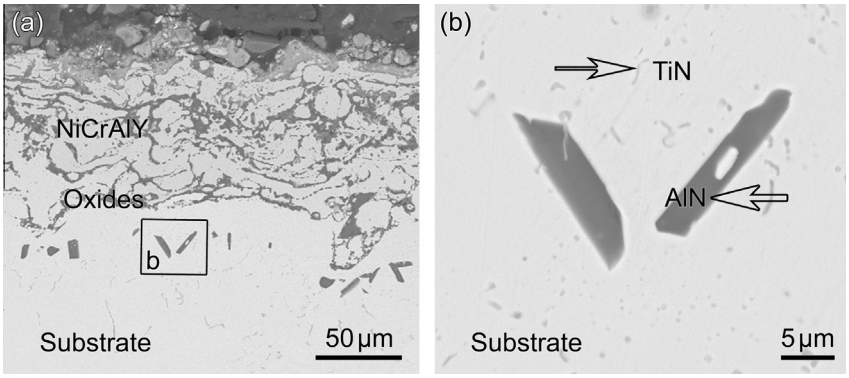

Fig. 5. Cross-sectional microstructures of the coating oxidized at 1100 °C for 25 h: (a) BEI of the integrate coating system, (b) local magnified image of the zone marked with "b" in (a), it clearly shows that TiN and AlN precipitate in the substrate.

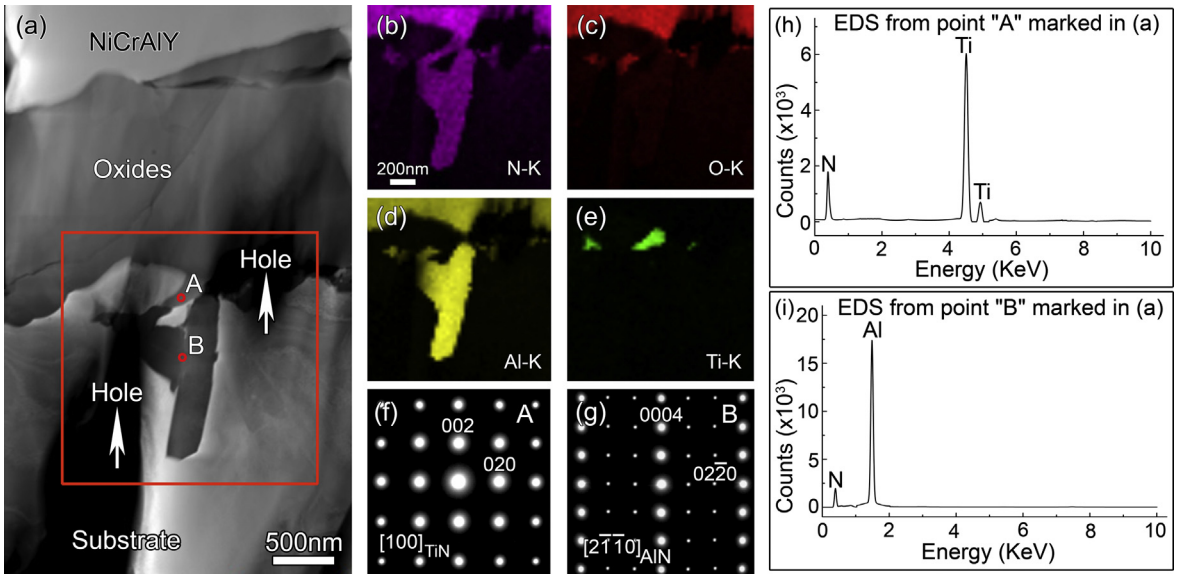

Fig. 6. Microstructure and chemical composition of the coating/substrate interface after oxidation at 1100 °C for 25 h: (a) HAADF image of the coating/substrate interface, (b)–(e) STEM-EDS maps from species of N, O, Al and Ti in the red frame in (a), respectively, (f) SAED of $[100]_{TiN}$ took from the precipitate marked with "A" in (a), (g) SAED of $[2\,\bar{1}\,\bar{1}\,0]_{AlN}$ took from the precipitate marked with "B" in (a), (h) and (i) EDS from point "A" and "B" marked in (a), respectively.

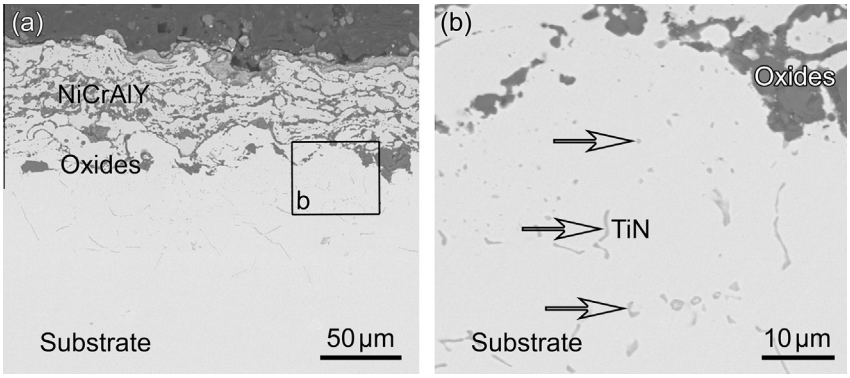

Fig. 7. Cross-sectional microstructures of the coating oxidized at 1100 °C for 50 h: (a) BEI of the integrate coating system, (b) local magnified image of the zone marked with "b" in (a), it clearly shows that only TiN precipitates remain in the substrate.

time, TiN remains and grows into deeper substrate interior (Fig. 7). As indicated by the corresponding STEM-EDS (Fig. 8b–g, h and i) and SAEDs (insets in Fig. 8a) in Fig. 8, in the substrate adjacent to the oxide layer, TiN and α-Al_2O_3 precipitates marked with "A" and "B" can be identified as TiN in [1 1 0] direction and α-Al_2O_3 in [0 0 0 1] direction, respectively.

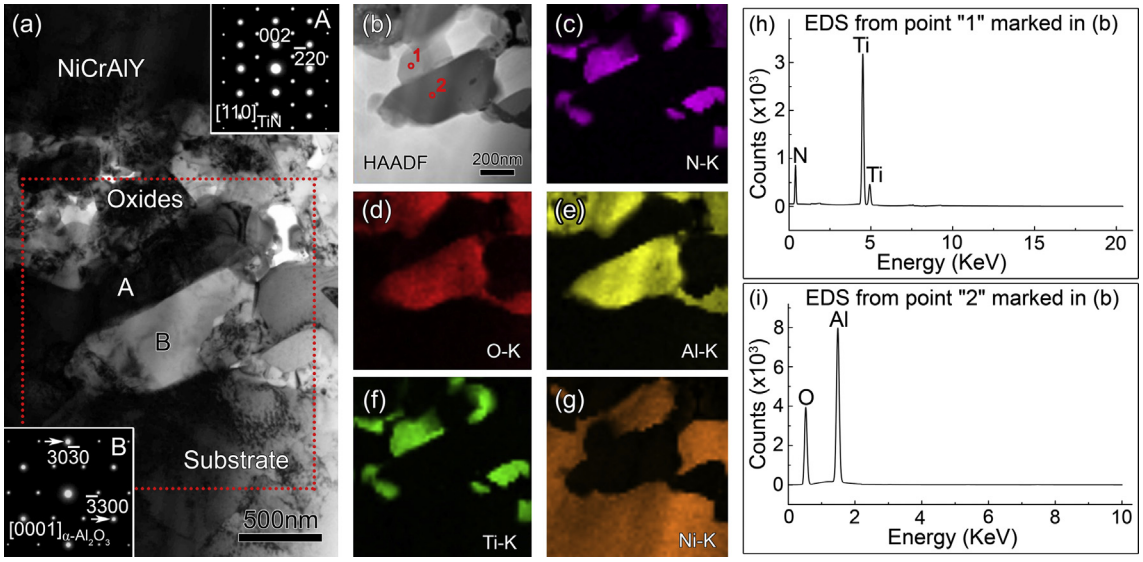

Fig. 8. Microstructure and chemical composition at the coating/substrate interface after oxidation at 1100 °C for 50 h: (a) BF image of the coating/substrate interface and SAEDs of TiN and α-Al_2O_3 which are took from [1 1 0] and [0 0 0 1], respectively, (b) HAADF image including partial oxides layer and the precipitate marked with "A" in (a), (c)–(g) STEM-EDS maps of N, O, Al, Ti, Cr and Ni, respectively, (h) and (i) EDS acquired from point "1" and "2" marked in (b), respectively.

The replacement of hcp-AlN with α-Al_2O_3 in the internal oxidation and nitridation zones corresponds to the reaction and local equilibrium as following:

$$2AlN + 3[O] = Al_2O_3 + 2[N]. \quad (8)$$

On one hand, at the present stage most of the easily oxidized elements in the coating has reacted with O, so O diffuses towards the substrate, providing enough O to react with the hcp-AlN. On the other hand, because the formation energy of α-Al_2O_3 (−1328 kJ/mol) is lower than that of AlN (−365.5 kJ/mol) at 1100 °C, the replacement reaction can take place between these phases under the $P_{O_2}^{3/2}/P_{N_2} \geqslant 1 \times 10^{-36}$ atm [23]. Due to these reasons, the Eq. (8) can be activated.

The reason for that TiN phase remains after 50 h oxidation is that the affinity between N and Ti (ΔH_f^{θ} (TiN) = 996.8 kJ/mol) is larger than that between O and Ti (ΔH_f^{θ} (TiO_2) = 677.5 kJ/mol; ΔH_f^{θ} (TiO) = 782.3 kJ/mol) at 1100 °C [20], so that N which generated from the Eq. (8) consequently reacts with Ti to form TiN under the same partial pressures of oxygen and nitrogen or even under lower nitrogen partial pressure than that of oxygen. As a result, the TiN grows further after 50 h oxidation at 1100 °C (Figs. 6–8).

3.6. Potential influence of the microstructural evolution on in-service mechanical behavior and improvement suggestions

The microstructural evolution revealed in this work may be harmful for the in-service mechanical behavior. First of all, phase changes could degrade the coating system. Such as formation of Al_2O_3, Al, AlN, and TiN accelerates the decomposition of γ′-Ni_3(Al,Ti) in the substrate, which will reduce the creep resistance of the superalloys. Furthermore, the new formed phases are harmful. Pure Al phase may lead to sudden crack of blades in service owing to its low melting point (~660 °C). Also, emergence of AlN and TiN precipitates generates grain boundaries and growth stress in the single crystal substrate, which enhances interdiffusion and increases velocity of crack growth, consequently deteriorate the high temperatures property of the superalloy [24].

Secondly, internal oxide layer may aggravate internal stress at the coating/substrate interface which could result in mechanical failure of the coating systems. For example, at the period of heating, tensile stress will occur in the oxide layer at the coating/substrate interface due to mismatch of coefficient of thermal expansion (CTE) among the oxide layer, NiCrAlY coating, and substrate; upon cooling, the CTE between the oxide layer, NiCrAlY coating, and substrate leads to a high compressive stress in the oxide layer. The complex stresses generated in service process provide the strain energy that can drive coating spallation, typically within and/or near the oxide layers [25]. Also, growth stress of the oxide layer during the internal oxidation also increases the risk of coating spallation [26]. Moreover, the sub-layer structure revealed in this work may make the stress in the oxide layer complicated and be destructive to the integrity of the coating/substrate interface even the whole coating system.

Finally, Kirkendall voids formed in the oxide layer owing to interdiffusion between the coating and the substrate can deteriorate the coating system. The Kirkendall voids, as shown in Fig. 2b, supply channels for further penetration of O and N into the substrate and consequently cause internal oxidation and nitridation in a deeper zone of the substrate. In addition, Kirkendall voids are one of key factors that reduce the adhesion of the coating/substrate interfaces and are responsible for a massive reduction in the fatigue strength of the coating system.

After 50 h oxidation, although significant microstructural evolution has emerged, risk of coating delamination is not high since the oxide layer is thin and the volume ratio of oxide and nitride in the substrate is small. However, with oxidation time extends, the risk will increase evidently. In order to control the risk, several suggestions could be considered. In terms of the coating composition design, reactive elements (RE) can be added to reduce the segregation of N, O and S at the coating/substrate interface [27,28]. In addition, suitable post-treatment process can be used to promote selective oxidation providing an ideal protective oxide scale [29], which can efficiently restrain the incessant penetration of N and O into the coating and the substrate. Moreover, a diffusion barrier layer can be brought into the coating/substrate interface to decrease the undesirable influence of interdiffusion. The barrier material systems include high-melting metals (W, Ir and Ru) [30] and ceramics (TiC, TiN, AlN, AlON and CrON) [31] which can efficiently block the

diffusion of O and/or N into the substrate and consequently prevent the internal oxidation and/or nitridation.

4. Conclusion

A NiCrAlY coating was vacuum plasma-sprayed on a Ni-based single crystal superalloy and then subjected to isothermal oxidation at 1100 °C in air up to 50 h. SEM and TEM were utilized to characterize the chemical and microstructural evolution of the coating/substrate interface. The internal oxidation and nitridation induced microstructural evolution of the coating/substrate interface was analyzed, leading to the following conclusions:

(1) Oxide layer comprising Cr_2O_3 and Al_2O_3 sub-layers forms at the coating/substrate interface after 5 h oxidation.
(2) Isothermal oxidation induces decomposition of γ'-Ni_3Al which results in precipitation of pure Al after 10 h oxidation.
(3) Hcp-AlN and fcc-TiN form in the substrate next to the oxides layer/substrate interface after 25 h oxidation.
(4) Hcp-AlN transforms into α-Al_2O_3 while fcc-TiN remains after 50 h oxidation.

At last, potential harmful influence of the microstructural evolution on mechanical behavior has been pointed out, and improvement methods also have been suggested.

Acknowledgments

This work was supported by the Major State Basic Research Development Program (973 Program) of China under grant No. 2010CB631206 and the "Hundred Talents Project" of Chinese Academy of Sciences, and from the National Natural Science Foundation of China (NSFC) (Nos. 50931004, 51071164, 51371173 and 50671102). We also greatly thank B. Wu and L.X. Yang for TEM assistance.

References

[1] N.P. Padture, M. Gell, E.H. Jordan, Thermal barrier coatings for gas-turbine engine applications, Science 296 (2002) 280–284.
[2] J.H. Perepezko, The hotter the engine, the better, Science 326 (2009) 1068–1069.
[3] R.C. Pennefather, D.H. Boone, Mechanical degradation of coating systems in high-temperature cyclic oxidation, Surf. Coat. Technol. 76 (1995) 47–52.
[4] M. Ranjbar-Far, J. Absi, G. Mariaux, F. Dubois, Simulation of the effect of material properties and interface roughness on the stress distribution in thermal barrier coatings using finite element method, Mater. Des. 31 (2010) 772–781.
[5] F. Cao, B. Tryon, C.J. Torbet, T.M. Pollock, Microstructural evolution and failure characteristics of a NiCoCrAlY bond coat in "hot spot" cyclic oxidation, Acta Mater. 57 (2009) 3885–3894.
[6] T.M. Pollock, D.M. Lipkin, K.J. Hemker, Multifunctional coating interlayers for thermal-barrier systems, MRS Bull. 37 (2012) 923–931.
[7] M. Hasegawa, T. Endo, H. Fukutomi, The effect of microstructure change of bond coat layer in air plasma-sprayed thermal barrier coating system on interfacial mechanical property under shear loading, J. Jpn. Inst. Met. 73 (2009) 802–808.
[8] M.M. Morra, R.R. Biederman, R.D. Sisson, Microstructural characterization of metallic overlay coatings by high-resolution analytical electron-microscopy, Thin Solid Films 119 (1984) 383–394.
[9] K. Zhang, Q.M. Wang, C. Sun, F.H. Wang, Preparation and oxidation behavior of NiCrAlYSi coating on a cobalt-base superalloy K40S, Corros. Sci. 50 (2008) 1707–1715.
[10] K.A. Unocic, B.A. Pint, Characterization of the alumina scale formed on a commercial MCrAlYHfSi coating, Surf. Coat. Technol. 205 (2010) 1178–1182.
[11] S.M. Jiang, C.Z. Xu, H.Q. Li, J. Ma, J. Gong, C. Sun, High temperature corrosion behaviour of a gradient NiCoCrAlYSi coating II: oxidation and hot corrosion, Corros. Sci. 52 (2010) 2316–2322.
[12] A.G. Evans, M.Y. He, A. Suzuki, M. Gigliotti, B. Hazel, T.M. Pollock, A mechanism governing oxidation-assisted low-cycle fatigue of superalloys, Acta Mater. 57 (2009) 2969–2983.
[13] L. Wang, Y. Wang, X.G. Sun, J.Q. He, Z.Y. Pan, Y. Zhou, P.L. Wu, Influence of pores on the thermal insulation behavior of thermal barrier coatings prepared by atmospheric plasma spray, Mater. Des. 32 (2011) 36–47.
[14] L. Wang, Y. Wang, X.G. Sun, J.Q. He, Z.Y. Pan, C.H. Wang, A novel structure design towards extremely low thermal conductivity for thermal barrier coatings — experimental and mathematical study, Mater. Des. 35 (2012) 505–517.
[15] B.W. Kempshall, Y.H. Sohn, S.K. Jha, S. Laxman, R.R. Vanfleet, J. Kimmel, A microstructural observation of near-failure thermal barrier coating — a study by photostimulated luminescence spectroscopy and transmission electron microscopy, Thin Solid Films 466 (2004) 128–136.
[16] B.M. Warnes, N.S. DuShane, J.E. Cockerill, Cyclic oxidation of diffusion aluminide coatings on cobalt base superalloys, Surf. Coat. Technol. 148 (2001) 163–170.
[17] W.Z. Li, Y.Q. Li, C. Sun, Z.L. Hu, T.Q. Liang, W.Q. Lai, Microstructural characteristics and degradation mechanism of the NiCrAlY/CrN/DSM11 system during thermal exposure at 1100 °C, J. Alloys Compd. 506 (2010) 77–84.
[18] J. Litz, A. Rahmel, M. Schorr, Selective carbide oxidation and internal nitridation of the Ni-base superalloys IN-738 LC and IN-939 in air, Oxid. Met. 30 (1988) 95–105.
[19] U. Krupp, H.J. Christ, Selective oxidation and internal nitridation during high-temperature exposure of single-crystalline nickel-base superalloys, Metall. Mater. Trans. A 31 (2000) 47–56.
[20] R.C. Weast, CRC Handbook of Chemistry and Physics, 85th ed., CRC Press, Washington, DC, Boca Raton, London, New York, 2004.
[21] H. Bohner, Under cooling of high melting intermetallic compounds in aluminium alloys, Z. Metallkd. 26 (1934) 268–271.
[22] W.L. Fink, L.A. Willey, Equilibrium relations in aluminum-nickel alloys of high purity, Trans. AIME 111 (1934) 293–303.
[23] S. Han, D.J. Young, Simultaneous internal oxidation and nitridation of Ni–Cr–Al alloys, Oxid. Met. 55 (2001) 223–242.
[24] J.X. Dong, K. Sawada, K. Yokokaw, F. Abe, Internal nitridation behavior during long-term creep in a nickel-base superalloy, Scripta Mater. 44 (2001) 2641–2646.
[25] W.Z. Li, Q.M. Wang, Z.B. Bao, Y. Yao, J. Gong, C. Sun, X. Jiang, Microstructural evolution of the NiCrAlY/CrON duplex coating system and its influence on mechanical properties, Mater. Sci. Eng., A 498 (2008) 487–494.
[26] J. Liu, J.W. Byeon, Y.H. Sohn, Effects of phase constituents/microstructure of thermally grown oxide on the failure of EB-PVD thermal barrier coating with NiCoCrAlY bond coat, Surf. Coat. Technol. 200 (2006) 5869–5876.
[27] A. Vande Put, M.C. Lafont, D. Oquab, A. Raffaitin, D. Monceau, Effect of modification by Pt and manufacturing processes on the microstructure of two NiCoCrAlYTa bond coatings intended for thermal barrier system applications, Surf. Coat Technol. 205 (2010) 717–727.
[28] M. Mobin, H.K. Sharma, S.K. Hasan, High temperature oxidation behaviour of CeO_2 and La_2O_3 modified aluminide coatings on carbon steel, Anti Corros. Methods Mater. 49 (2002) 283–294.
[29] K. Fritscher, Y.T. Lee, Investigation of an as-sprayed NiCoCrAlY overlay coating – microstructure and evolution of the coating, Mater. Corros. 56 (2005) 5–14.
[30] D. Sumoyama, K.Z. Thosin, T. Nishimoto, T. Yoshioka, T. Izumi, S. Hayashi, T. Narita, Formation of a rhenium-base diffusion-barrier-coating system on Ni-base single crystal superalloy and its stability at 1423 K, Oxid. Met. 68 (2007) 313–329.
[31] J. Muller, D. Neuschutz, Efficiency of alpha-alumina as diffusion barrier between bond coat and bulk material of gas turbine blades, Vacuum 71 (2003) 247–251.